**RESEARCH ARTICLE** `OPEN ACCESS`

# A Closer Look at the FeS Heme Bonds in *Azotobacter vinelandii* Bacterioferritin: QM/MM and Local Mode Analysis

Marek Freindorf | Elfi Kraka [ORCID]

Chemistry Department, Southern Methodist University, Dallas, Texas

**Correspondence:** Elfi Kraka (ekraka@gmail.com)

## ABSTRACT

Using the QM/MM methodology and a local mode analysis, we investigated a character and a strength of FeS bonds of heme groups in oxidized and reduced forms of Bacterioferritin from *Azotobacter vinelandii*. The strength of the FeS bonds was correlated with a bond length, an energy density at a bond critical point, and a charge difference of the F and S atoms. Changing the oxidation state from ferrous to ferric generally makes the FeS bonds weaker, longer, more covalent, and more polar. We also investigated the SFeS bond bending and found that the stronger FeS bond, generally makes the SFeS bond bending stiffer, which could play a key role in the balance between ferric and ferrous oxidation states and related biological activities.

## 1 | Introduction

Iron is an essential element in metalloproteins, which are involved in important biochemical processes such as oxygen transport and storage, synthesis of amino acids and DNA, and other metabolic processes involving electron transfer and catalysis [1]. The biochemical activity of iron is related to its ability to form organometallic complexes and the ability of easily switching between the ferric ($Fe^{3+}$) and the ferrous ($Fe^{2+}$) oxidation states under physiological conditions [2]. However, an unbalance between the ferric and ferrous states, in particular the excess of $Fe^{2+}$ ions in living organisms, can lead to the formation of harmful oxygen-derived free radicals, which can cause a wide range of damage such as tissue injury or oxidative DNA damage, just to name a few [3–6]. A family of proteins called ferritins serve as iron reservoir, and also regulate the proper balance between the ferric and ferrous iron [7]. They sequester excess of intracellular iron and store insoluble clusters of redox-inactive ferric $Fe^{3+}$ ions in a nano-cage embedded inside the protein, a process termed *biomineralization* of iron [8–11]. In the case of a ferrous iron

deficiency or high demand, they reduce insoluble ferric $Fe^{3+}$ iron to its soluble ferrous $Fe^{2+}$ form and release it as needed [3–5].

A subfamily of ferritins found in bacteria, called bacterioferritins (BFs), differs from other family members by the presence of heme groups binding two protein chains at the interface of two monomers via chemical bonds with two methionine amino acids [12–17]. BFs form spherical, hollow structures assembled from 24 protein subunits (ca. 120 Å outer diameter, and ca. 80 Å inner diameter) [17]. The structures may be different for the different iron oxidation states, as it has been shown in x-ray studies of the oxidized and reduced forms of the native *Azotobacter Vinelandii* bacterioferritin (AvBF) [18, 19]. AvBF has three iron-containing sites within the protein, namely an iron dinuclear site, a heme group of the b-type [18, 19], and a single iron atom in the protein shell, with the dinuclear iron site of AvBF being the main reaction site responsible for the ferroxidase reaction [19]. However, a number of experimental studies have shown the importance of the other two sites for additional BFs activities, and particular for the controlled iron release from the BFs

iron biomineral storage [15, 17, 20–34]. The reduction of $Fe^{3+}$ and subsequent release from the BF requires the interaction between BF and a small protein ferredoxin (BFd), which transfers electrons to the internal cavity of BF in order to reduce the $Fe^{3+}$ to $Fe^{2+}$ ions for subsequent release. The heme groups of BF mediate the electron transfer between the dinuclear iron cluster of BFd and $Fe^{3+}$ of the BF mineral core. Blocking the interaction between BF and BFd via small molecule inhibitors, allows to manipulate the balance between the $Fe^{3+}$ and $Fe^{2+}$ ions in BF, and can lead to irreversible accumulation of $Fe^{3+}$ in BF leading to bacterial cell death, which opens new design routes for potential antibiotics [28, 31, 34].

A necessary prerequisite for a systematic exploration of these new design routes is a better understanding of the heme-BF bonding for both the ferric and the ferrous states at a molecular level, which to our best knowledge has so far been missing. As a first important step in this direction, the major objective of this study has been to assess and compare for both the ferric and the ferrous oxidation states, the strength of the heme FeS chemical bonds connecting each of the four characteristic, symmetrically non-equivalent protein chain pairs AB, CD, EF, and GH, (see Figure 1a,b), which have been identified via x-ray [19].

As sketched in the insert of Figure 1b for the protein chain pair AB, the two protein chains are connected via FeS bonding between the heme iron and sulfur atoms of two methionines (Met52 of the chain A, and Met52′ of the chain B). We utilized for the calculations a hybrid QM/MM (quantum mechanics – molecular mechanics) ansatz [36–40], applied to different protein fragments, as well to a gas phase model depicted in Figure 2. For the FeS bond strength assessment we used the local vibrational mode theory developed in our group [41, 42], complemented with Bader's quantum theory of atoms in molecules (QTAIM) analysis [43–45], and the natural bond orbital (NBO) analysis [46, 47]. A particular focus of this work was
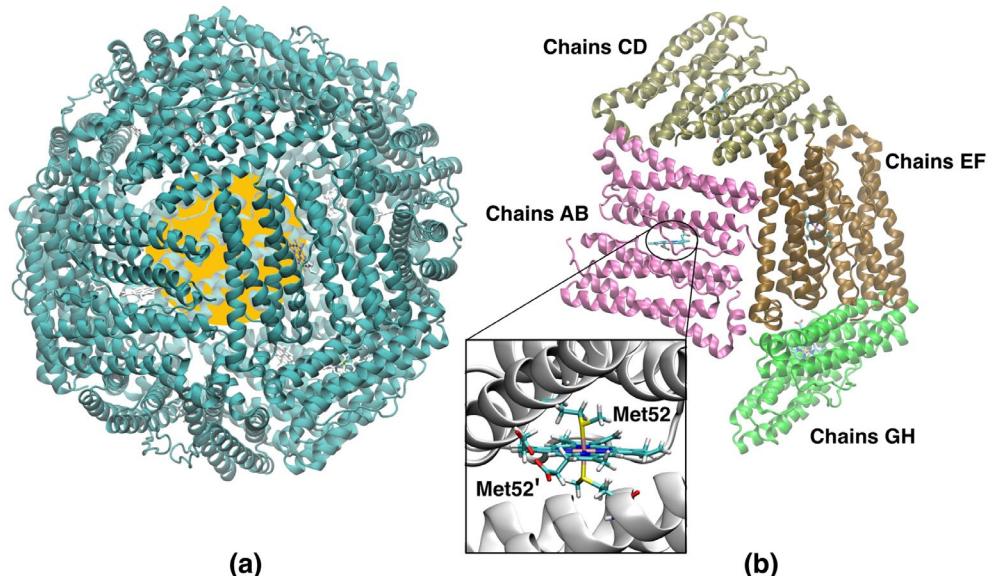


**FIGURE 1** | (a) Sketch of Bacterioferritin with iron mineral core (in yellow) based on x-ray protein structure PDB entry 1BFR [35]. (b) Selected protein chains investigated in this study where insert shows one heme group coordinated to side chains of two methionines, from x-ray protein structure PDB entry 2FKZ [19].
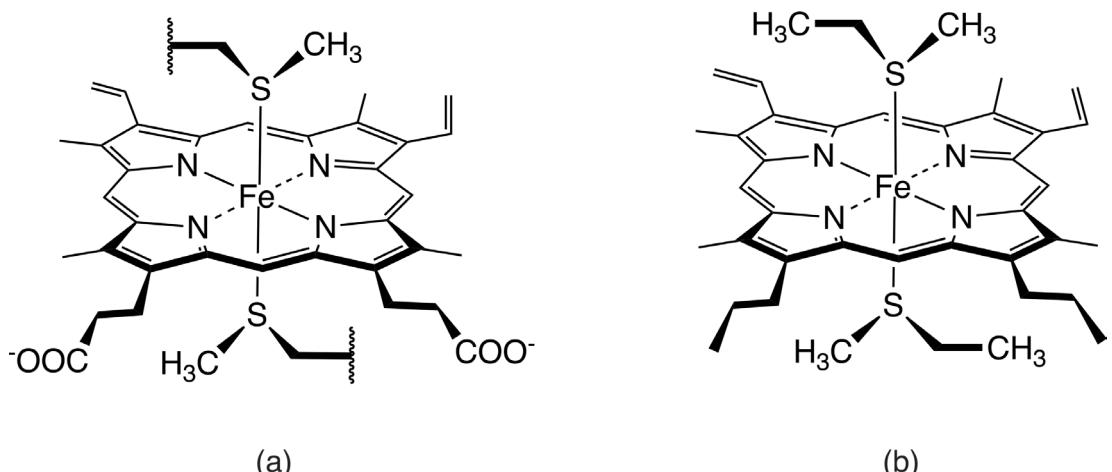


**FIGURE 2** | Computational models of heme group used in calculations of bacterioferritin in this study. (a) QM model in QM/MM calculations. (b) QM model in gas phase calculations.

to analyze how different heme sites of AvBF show different FeS bond strengths in different iron oxidation states, which in turn can influence the biochemical activity in both the ferric and the ferrous protein forms.

## 2 | Methodology

Starting coordinates of the BF protein were taken from the x-ray structure of AvBF for both the oxidized and the reduced forms (PDB entries: 2FKZ and 2FL0, respectively) [19]. The experimental structure was divided in our study into four protein dimers, each including two protein chains for each oxidation form (**ABo**, **CDo**, **EFo**, and **GHo**, for the oxidized protein, and **ABr**, **CDr**, **EFr**, and **GHr**, for the reduced protein). Each protein dimer was formed from two chains bound together by one heme group, as depicted in the insert of Figure 1b for the protein chain pair AB. Each dimer was calculated separately using the same QM/MM computational protocol, which is explained in the following.

Hydrogen atoms were added using the AMBER program with the force field ff19SB [48], and the protein dimer was surrounded by a water sphere of TIP3P water molecules [49] with a radius of 16 Å, centered at the Fe atom of the heme group. The parameters for the heme group were taken from Giammona's Ph.D. thesis [50]. The protein dimer was neutralized by $Na^+$ counter-ions and was energetically minimized with AMBER. The minimized structure was then divided into a QM part, which includes the heme group and side chains of two methionines (see Figure 2a), (95 QM atoms) while the MM part includes the rest of the protein dimer (5315 MM atoms). QM/MM calculations, including geometry optimization and frequency calculation, were performed using the ONIOM method with mechanical embedding using the standard optimization criterion, followed by scaled electronic embedding using the smaller step size of the value of 0.05 Bohr or radians [51]. In order to avoid overestimation of the electrostatic interactions between QM and MM atoms and overpolarization of the QM electron density by the closest point charges from the MM part [52, 53], we have scaled charges of the MM atoms separated from the QM atoms at the distance smaller than six bond lengths, by 40%, as implemented in the ONIOM method. The optimized geometries of all protein dimers investigated in our study, were identified as minima on the potential energy surface (PES), which was confirmed by vibrational frequency calculations. The QM/MM calculations were performed with the PBE0/6-31G(d,p)/AMBER level of theory [54, 55], while the calculations in the gas phase (see Figure 2b) were done with the PBE0/6-31G(d,p) level of theory. The calculations for the ferric state of the protein and the gas phase models, were performed in the doublet electronic state, while for the ferrous state in the singlet electronic state, as suggested by an experimental study [56]. The PBE0 functional was used because it is well fitted for transition metals complexes [54, 57–59], and has been successfully used in our previous QM/MM calculations of hemoproteins [60]. The choice of the PBE0 functional was also supported by another computational study [61], showing that this functional is one of the best from a series of DFT functionals (BP86, PBE, PBE0, TPSS, TPSSH, B3LYP, and B97-D) for calculations of iron porphyrin complexes in the gas phase. Moreover, according to our test calculations with the PBE0/6-31G(d,p) level of theory, the calculated FeN bond length

(1.965 Å) of a bishistidyl model of the heme group, is close to the experimental x-ray FeN bond distance in bis(1-methylimidazole) (meso-tetramesitylporphinato) Fe(III) (1.970 Å) [62].

Local mode force constants $k^a$ can be transformed into relative bond strength orders (BSO) via a power relationship of the form $BSO = A * (k^a)^B$ according to the generalized Badger rule derived by Cremer, Kraka, and co-workers [63, 64]. The parameters A and B are obtained from two reference molecules with known BSO and $k^a$ values. Because the chemical bonds investigated in this study involve a transition metal, we used the corresponding Mayer's bond orders [65–67]. The reference molecule for a single bond with the metal was $CuCH_3$ ($k^a = 3.243$ mDyn/Å, BSO = 1.005), and for a double bond $NiCH_2$ ($k^a = 5.568$ mDyn/Å, BSO = 1.894). Based on the interpolation, the power relationship parameters are $A = 0.2530$ and $B = 1.1724$.

The intrinsic strength of the FeS chemical bonds in the protein dimers and gas phase model for both oxidation states was determined with Local Mode Analysis (LMA) developed in our group. Mathematical details, a history of LMA, and a summary of wide-spread LMA applications can be found in two comprehensive review articles [41, 42]. LMA has evolved over the years into a versatile computational instrument, facilitating the extraction of critical chemical insights from vibrational spectroscopy data. Normal vibrational modes of a polyatomic molecule are generally delocalized, as stated by Wilson in 1941 via his proof that the associated normal mode coordinates **Q** is a linear combination of internal coordinates **q** or Cartesian coordinates **x** [68]. Therefore, normal vibrational modes are generally delocalized over a molecule and normal mode stretching frequencies and associated stretching force constants are of limited use as individual bond strength descriptors. Konkoli and Cremer solved this problem via the transformation of normal vibrational modes into their local mode counterparts [69, 70]. A local vibrational mode $\mathbf{a}_n$ is defined as

$$\mathbf{a}_n = \frac{\mathbf{K}^{-1}\mathbf{d}_n^\dagger}{\mathbf{d}_n\mathbf{K}^{-1}\mathbf{d}_n^\dagger} \qquad (1)$$

Important to note is that the two ingredients needed for LMA, the diagonal normal mode force constant matrix **K** in normal mode coordinates **Q** and the normal mode vectors $\mathbf{d}_n$ in internal coordinates, can be obtained from a vibrational frequency calculation via the Wilson GF formalism [68, 71], which is a routine part of most modern quantum chemistry packages [72]. That means, LMA can be applied with minimal computational costs after a routine quantum-chemical calculation of vibrational frequencies, optionally adding measured frequencies as input (a feature opening LMA to experimental vibrational spectroscopists) to single molecules in the gas phase, solution, or in a protein, but also to periodic systems such as crystals [41, 42].

For each local mode $\mathbf{a}_n$, one can derive associated local force constants $k_n^a$ describing the local vibration of the atomic fragment under consideration,

$$k_n^a = \mathbf{a}_n^\dagger \mathbf{K} \mathbf{a}_n = \frac{1}{\mathbf{d}_n\mathbf{K}^{-1}\mathbf{d}_n^\dagger} \qquad (2)$$

local mode frequencies, local mode infrared intensities, and other local properties [42, 73]. Another important feature of LMA is the characterization of the normal mode (CNM) procedure, which decomposes each normal vibrational mode into local mode contributions [41, 42, 74, 75]. CNM has advanced the interpretation of vibrational spectra to the next level, for example, identifying which molecular fragments couple in DNA-base pairs, or assessing the quality of Stark effect probes with a local probe bond, just to name two examples [76–79]. In this work we will predominantly focus on local mode stretching force constants $k_n^a(AB)$ reflecting the intrinsic strength the bond/interaction between two atoms A and B [80]. Over the past two decades, we have successfully applied local mode force constants to characterize the strength of covalent bonds and non-covalent interactions across the periodic table as documented in [41, 42] including bonding inside active sites of proteins [60, 77, 81–86].

We complemented LMA with features of the analysis of the electron density $\rho(\mathbf{r})$ via Bader's QTAIM theory [43–45]. In particular the covalent character of the FeS bonds were determined via the Cremer–Kraka criterion [87, 88] of covalent bonding, which is based on the energy density $H(\mathbf{r}) = G(\mathbf{r}) + V(\mathbf{r})$, where the kinetic energy density is $G(\mathbf{r})$ (positive, destabilizing) and the potential energy density is $V(\mathbf{r})$ (negative, stabilizing). If at the bond critical point $\mathbf{r}_b$ of $\rho(\mathbf{r})$ between two bonded atoms AB $H(\mathbf{r}_b)$ is negative, the character of AB bond is predominantly covalent, whereas a positive $H(\mathbf{r}_b)$ value indicates a predominantly electrostatic character. In addition we analyzed the Fe and S NBO atomic charges [46, 89]. QM/MM calculations were performed with the Gaussian16 program [90], LMA calculations with the LModeA program package [91], QTAIM calculations with AIMALL [92], and NBO charges were calculated utilizing the NBO analysis implemented in Gaussian program. Pictures of QM/MM optimal geometries of heme groups and gas phase models of the investigated molecular systems, along with their Cartesian coordinates are presented in Supporting Information. The comparison between the calculated and the experimental

heme geometrical parameters (bonds and angles) for the investigated protein-chain dimers have been included in Supporting Information.

## 3 | Results and Discussion

The results of our analysis for the FeS chemical bonds in AvBF are presented in Table 1 for the ferric oxidation state and in Table 2 for the ferrous state, showing the local mode bond length R, the local mode force constant $k^a$, the local mode frequency $\omega^a$, the energy density at a bond critical point $H_\rho$, the Fe and S atomic charge difference, and the bond strength order BSO. The bond labels in our study use the following notation, for example, **ABoa** denotes the FeS chemical bond of the AB protein chains, in the oxidized (ferric) state, and for the heme pocket which corresponds to Met52 coordinated to the heme group. However **ABob** denotes the FeS bond for the same protein chains, in the same oxidation state, but for the opposite heme pocket linking the heme group with Met52′. **ABra** and **ABrb** denote the same two bonds in the reduced (ferrous) state. Similar notation is used for the CD, EF, and GH protein chains, while GAS denotes the FeS bond calculated in the gas phase. The plots of the properties of the FeS chemical bonds in AvBF and the gas phase models are presented in Figures 3 and 4. The strength of the FeS chemical bonds in the ferric state of AvBF is presented in Figure 3a. The majority of the FeS bonds in this state (the average $k^a = 0.436$ mDyn/Å, for **ABoa**, **ABob**, **CDoa**, **CDob**, **EFoa**, and **EFob**) are weaker than in the gas phase (the average $k^a = 0.621$ mDyn/Å, for **GASoa** and **GASob**). The exceptions are the bonds in the GH chains (the average $k^a = 0.803$ mDyn/Å, for **GHoa** and **GHob**). The weakest FeS bond is found in our study for the EF protein chains (**EFoa**, $k^a = 0.359$ mDyn/Å), while the strongest for the GH chains (**GHoa**, $k^a = 0.879$ mDyn/Å). The strength of the FeS chemical bonds in the ferrous state of AvBF are presented in Figure 3b. According to Figure 3b, the FeS bonds in the protein (the average $k^a = 0.696$ mDyn/Å) are stronger than in the gas phase (the average $k^a = 0.544$ mDyn/Å), which is opposite to the strength of this

**TABLE 1** | Local mode bond length R, local mode force constant $k^a$, local mode frequency $\omega^a$, energy density at a bond critical point $H_\rho$, Fe and S atomic charge difference $\Delta Q$, and bond strength order BSO of FeS chemical bond, in ferric state of AvBF. For labels see the text.

| Bond | R | $k^a$ | $\omega^a$ | $H_\rho$ | $\Delta Q$ | BSO |
|---|---|---|---|---|---|---|
| | Å | mDyn/Å | cm$^{-1}$ | Hartree/Bohr$^3$ | e | |
| **ABoa** | 2.364 | 0.463 | 197 | −0.0182 | 0.576 | 0.103 |
| **ABob** | 2.371 | 0.436 | 191 | −0.0180 | 0.570 | 0.096 |
| **CDoa** | 2.372 | 0.422 | 188 | −0.0160 | 0.603 | 0.092 |
| **CDob** | 2.358 | 0.445 | 193 | −0.0162 | 0.592 | 0.098 |
| **EFoa** | 2.412 | 0.359 | 173 | −0.0151 | 0.598 | 0.076 |
| **EFob** | 2.355 | 0.492 | 203 | −0.0181 | 0.572 | 0.110 |
| **GHoa** | 2.366 | 0.879 | 271 | −0.0194 | 0.572 | 0.217 |
| **GHob** | 2.400 | 0.726 | 246 | −0.0174 | 0.591 | 0.174 |
| **GASoa** | 2.381 | 0.632 | 230 | −0.0176 | 0.562 | 0.148 |
| **GASob** | 2.386 | 0.609 | 225 | −0.0173 | 0.566 | 0.141 |

**TABLE 2** | Local mode bond length R, local mode force constant $k^a$, local mode frequency $\omega^a$, energy density at a bond critical point $H_\rho$, Fe and S atomic charge difference $\Delta Q$, and bond strength order BSO of FeS chemical bond, in ferrous state of AvBF. For labels see the text.

| Bond | R | $k^a$ | $\omega^a$ | $H_\rho$ | $\Delta Q$ | BSO |
|------|------|---------|-------------|------------------------|------|------|
|      | Å | mDyn/Å | cm$^{-1}$ | Hartree/Bohr$^3$ | e | |
| ABra | 2.326 | 0.764 | 252 | −0.0136 | 0.388 | 0.185 |
| ABrb | 2.346 | 0.692 | 240 | −0.0131 | 0.394 | 0.164 |
| CDra | 2.363 | 0.619 | 227 | −0.0112 | 0.413 | 0.144 |
| CDrb | 2.327 | 0.755 | 251 | −0.0131 | 0.395 | 0.182 |
| EFra | 2.335 | 0.736 | 248 | −0.0117 | 0.391 | 0.177 |
| EFrb | 2.334 | 0.732 | 247 | −0.0129 | 0.389 | 0.175 |
| GHra | 2.343 | 0.679 | 238 | −0.0128 | 0.399 | 0.161 |
| GHrb | 2.368 | 0.589 | 222 | −0.0106 | 0.417 | 0.136 |
| GASra | 2.364 | 0.548 | 214 | −0.0107 | 0.397 | 0.125 |
| GASrb | 2.367 | 0.539 | 212 | −0.0105 | 0.400 | 0.123 |
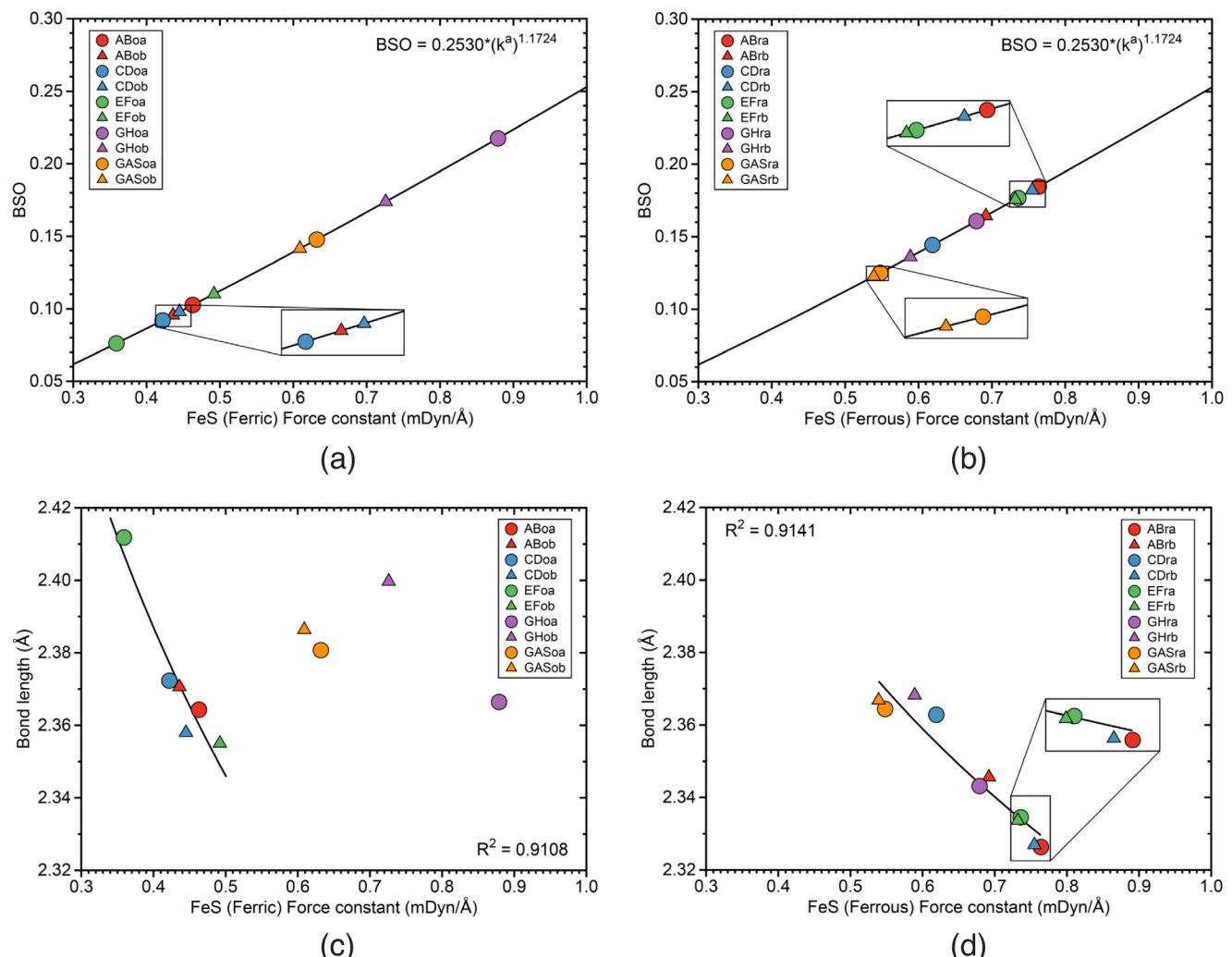


**FIGURE 3** | Properties of FeS chemical bonds in AvBF and gas phase models. (a) Relationship between local mode force constant $k^a$ and BSO for ferric state. (b) Relationship between local mode force constant $k^a$ and BSO for ferrous state. (c) Relation between local mode force constant $k^a$ and bond length R for ferric state. (d) Relation between local mode force constant $k^a$ and bond length R for ferrous state. For molecular labels, see the text.
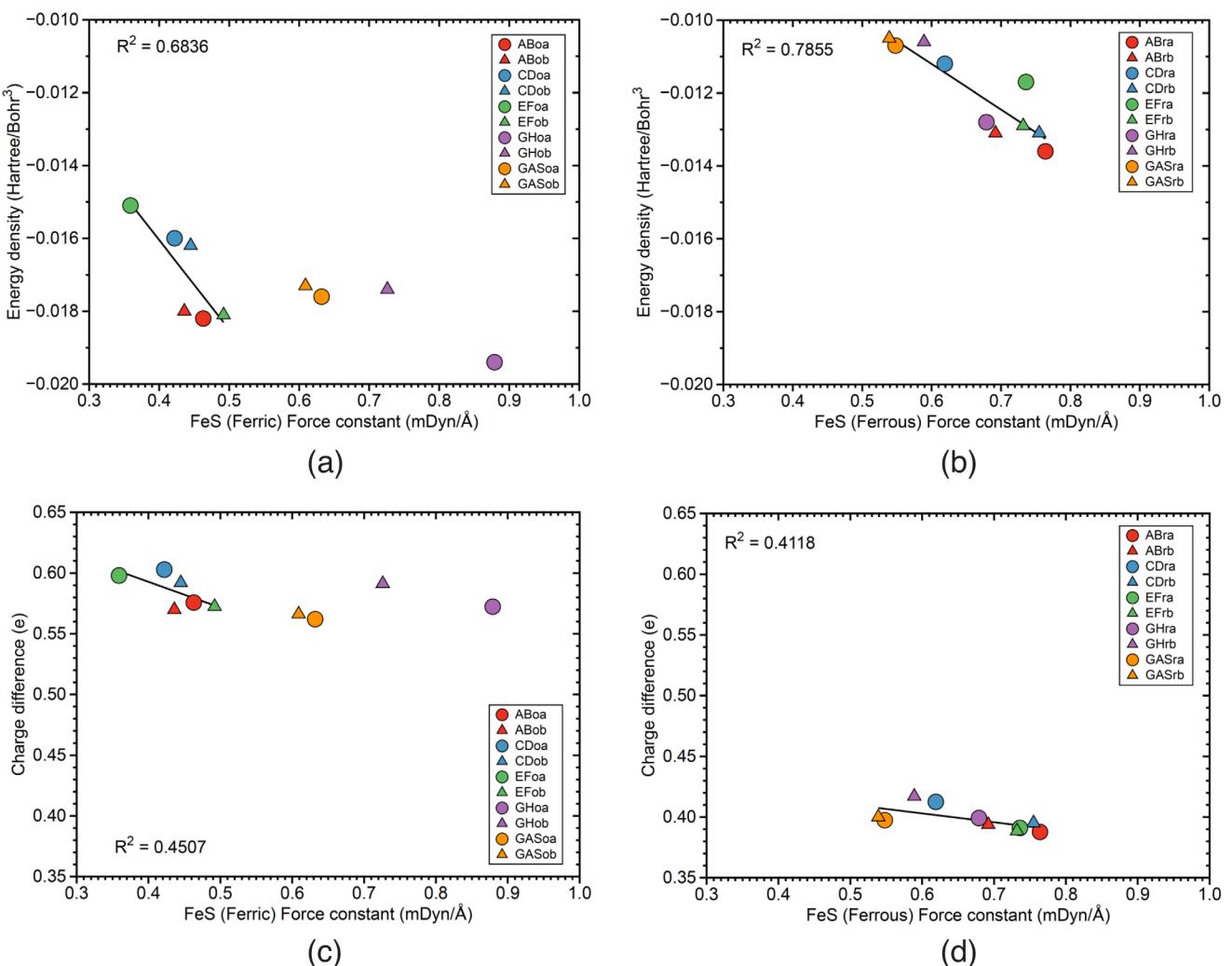
**FIGURE 4** | Properties of FeS chemical bonds in AvBF and gas phase models. (a) Relation between local mode force constant $k^a$ and energy density at bond critical point for ferric state. (b) Relationship between local mode force constant $k^a$ and energy density at bond critical point for ferrous state. (c) Relation between local mode force constant $k^a$ and charge difference for ferric state. (d) Relation between local mode force constant $k^a$ and charge difference for ferrous state. For molecular labels, see the text.

bond in the ferric state. The weakest bond in the ferrous state of the protein is for the GH chain ($k^a = 0.589$ mDyn/Å, for **GHrb**), while the strongest is for the AB chain ($k^a = 0.764$ mDyn/Å, for **ABra**). Generally, we found in this study that the strength of the FeS bond in the ferric state of the protein, is smaller than in the gas phase, with the exception of the GH protein chain showing the opposite change of the bond strength.

The change of the FeS bond strength in the protein relative to the gas phase, is mainly caused by two effects. The first effect is related to the change in the electronic structure of the heme group, which is induced by the electrostatic field of the heme pocket, and is also induced by non-bonding interactions between the heme group and side chains of the heme pocket. The second effect is related to constraints formed by the protein backbone on side chains of the methionine amino acids, which are bonded to Fe of the heme group, and both effects make the FeS bond in the protein weaker than in the gas phase. The opposite effect is observed in our calculations for the ferrous state, where the strength of this bond in the protein is bigger than in the gas phase, indicating the reverse effects of the protein environment

on the FeS bond strength. It is also interesting to note that in the gas phase the strength of the FeS bond in the ferric state, is bigger than the strength of this bond in the ferrous state. However in the protein, the change of the strength in the FeS bond is opposite, and in the ferric state of the protein, this bond is generally weaker than in the ferrous state.

Figure 3c,d, show the correlations between the local mode force constants $k^a$ and the bond length R, in the ferric and ferrous states. According to Figure 3c the strength of the FeS bonds in the ferric state of the chains AB, CD, and EF is relatively well correlated with the bond length ($R^2 = 0.9108$), which follows a general rule that a stronger bond is shorter, based on the Badger power relationship between them [64, 93]. However, according to our results, the FeS bonds in the GH protein chain and in the gas phase are outliners in the correlations for this oxidation state. The average bond length in the ferric state for the AB, CD, and EF protein chains (R = 2.372 Å), is similar to the average bond length in the gas phase (R = 2.384 Å), and to the average bond length for the GH protein chain (R = 2.383 Å). According to Figure 3d, all investigated FeS bonds in the ferrous state, follow the general

rule showing a relatively good correlation between the bond strength and the bond length ($R^2 = 0.9141$). The average bond length in the ferrous state of the protein (R = 2.343 Å) is smaller than the average bond length in the gas phase (R = 2.366 Å). Generally, we observed that the average FeS bond length in the ferric state of the protein (R = 2.372 Å) is bigger than in the ferrous state (R = 2.343 Å), which is also consistent with the Badger rule saying that the strength of this bond in the ferric state ($k^a = 0.436$ mDyn/Å) is smaller than in the ferrous state ($k^a = 0.696$ mDyn/Å). However in the gas phase, the average FeS bond length in the ferric state (R = 2.383Å) is bigger than in the ferrous state (R = 2.366 Å), but the average strength of this bond in the ferric state ($k^a = 0.803$ mDyn/Å) is also bigger than in the ferrous state ($k^a = 0.544$ mDyn/Å), which shows the exception from the Badger rule.

Figure 4a,b present a correlation between the local mode force constant $k^a$ and the energy density at a bond critical point $H_\rho$ in the ferric and ferrous states. Because, we observe in our study that in the ferric state of AvBF, there is a correlation between the local mode force constant and the bond length of the FeS bond only for AB, CA, and EF protein chain pairs (see Figure 3c), therefore we limit the correlations of the other bond properties of this bond to these protein pairs. According to Figure 4a there is a relatively weak correlation between the local mode force constant and the energy density at a bond critical point ($R^2 = 0.6836$) for the selected protein chains, where the GH protein chains and GAS are still outliners. The average energy density in the ferric state of the selected chains ($H_\rho = -0.0169$ Hartree/Bohr$^3$) is slightly less negative than in the gas phase ($H_\rho = -0.0174$ Hartree/Bohr$^3$), which indicates on a less covalent character of this bond in the protein. However, in the ferrous state the correlation between the local mode force constant and the energy density is better ($R^2 = 0.7855$) but still not perfect, and the average energy density in the ferrous state ($H_\rho = -0.0124$ Hartree/Bohr$^3$) is more negative than in the gas phase ($H_\rho = -0.0106$ Hartree/Bohr$^3$), showing the opposite protein effect. Comparing the average energy density of the FeS bond in the protein between the ferrous state ($H_\rho = -0.0124$ Hartree/Bohr$^3$) and the ferric state ($H_\rho = -0.0169$ Hartree/Bohr$^3$), we can conclude that oxidation process of the protein leads to a more covalent character of this bond, however the bond becomes generally weaker (the average value of $k^a = 0.696$ and 0.436 mDyn/Å, for the ferrous

and ferric state, respectively). Here it is important to notice that the energy density at a bond critical point, shows the covalent character of a chemical bond, but only in one point on the potential energy surface. However, the local mode force constant is based on a local mode covering a much bigger area of the potential energy surface, giving a much more accurate value of the bond strength.

Figure 4c,d show a correlation between the local mode force constant $k^a$ and the charge difference between the Fe and S atoms $\Delta Q$ in the ferric and ferrous states. In the ferric state, we limit the correlation between these bond properties to the selected protein chains AB, CD, and EF, as we have done it in the previous bond properties of this study. According to Figure 4c, there is a relatively weak correlation ($R^2 = 0.4507$) of these bond properties in the ferric state, and the average charge difference in the protein ($\Delta Q = 0.585$ e) is slightly bigger than in the gas phase ($\Delta Q = 0.564$ e), indicating on a slightly bigger polarization of the electron density in this bond, which is induced by the protein surrounding. According to Figure 4d, in the ferrous state the correlation between the local mode force constant and the charge difference has a similar quality ($R^2 = 0.4118$), and the average charge difference in the protein ($\Delta Q = 0.398$ e) is similar as in the gas phase ($\Delta Q = 0.399$ e). Generally, we observe in our study, that the oxidation process of the protein, is increasing the charge difference (the average value of $\Delta Q = 0.398$ and 0.585 e, for the ferrous and ferric state, respectively) and it is making the FeS bond generally weaker (the average value of $k^a = 0.696$ and 0.436 mDyn/Å, for the ferrous and ferric state, respectively).

LMA is a powerful tool to derive a computational descriptor of the strength of chemical bonds and non-bonded interactions via local vibrational stretching force constants $k^a$(AB) [41, 42]. However, it also offers a tool for the assessment of the stiffness of bond angles via local bending mode force constants $k^a$(ABC), which we recently explored to assess the stiffness of the Cp-M-Cp (cyclopentadienyl-metal-cyclopentadienyl) bridging motifs in ansa-metallocenes [94]. Table 3 shows the values of the bond angle $\alpha$, the local mode force constant $k^a$, and the local mode frequency $\omega$ for the SFeS bond bending in both the ferric and the ferrous oxidation state of the protein chains and the gas phase model. Figure 5a,b present the correlations between the average local mode force constant of the FeS bonds

**TABLE 3** | Local mode bond angle $\alpha$, local mode force constant $k^a$, local mode frequency $\omega^a$ of the SFeS bending mode, in ferric and ferrous state of AvBF protein chains and gas phase model. For labels see the text.

| Label | Ferric | | | Label | Ferrous | | |
|---|---|---|---|---|---|---|---|
| | $\alpha$ | $k^a$ | $\omega^a$ | | $\alpha$ | $k^a$ | $\omega^a$ |
| | Degree | mDyn/Å | cm$^{-1}$ | | Degree | mDyn/Å | cm$^{-1}$ |
| **ABo** | 169 | 0.166 | 194 | **ABr** | 167 | 0.187 | 206 |
| **CDo** | 170 | 0.163 | 192 | **CDr** | 170 | 0.185 | 204 |
| **EFo** | 172 | 0.161 | 191 | **EFr** | 171 | 0.191 | 208 |
| **GHo** | 167 | 0.172 | 197 | **GHr** | 169 | 0.179 | 201 |
| **GASo** | 170 | 0.100 | 151 | **GASr** | 171 | 0.146 | 182 |
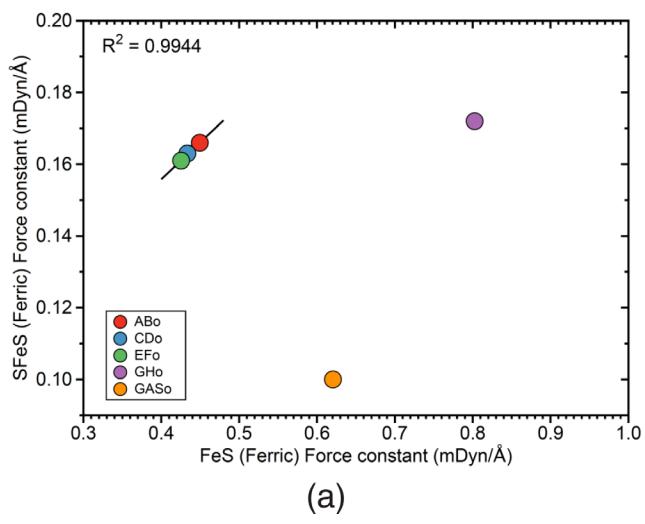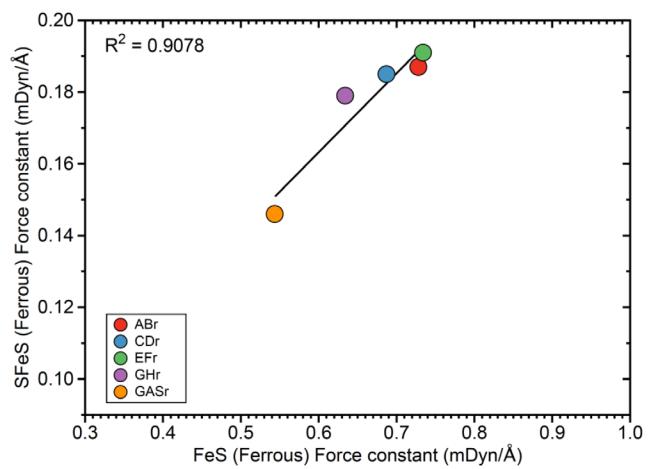
**FIGURE 5** | Correlation between average local mode force constants of FeS bonds and local mode force constants of SFeS bond bending in AvBF and gas phase models. (a) For ferric state. (b) For ferrous state. For molecular labels, see the text.

(for example the value of **ABo** for the FeS bond is an average value of the **ABoa** and **ABoa** bonds) in the selected protein chains, and the local mode force constant of the SFeS bond bending of the corresponding protein chains. Consequently to our analysis of the FeS bonds in the ferric state, there is a correlation between the local mode force constant of the FeS bond in this state, and the local mode force constant of the SFeS bond bending (see Figure 5a, $R^2 = 0.9944$) for the protein chain pairs AB, CD and EF, while the protein chain pair GH as well the gas phase model are the outliners. For the ferrous state, we observe a relatively good correlation (see Figure 5b, $R^2 = 0.9078$) between the local mode force constants related to the FeS bond and the SFeS bond bending. The correlations between the local mode force constants in both the ferric and the ferrous state presented in Figure 5a,b, show that stronger FeS bonds are related to stronger SFeS bond bending. However, according to our analysis, there is no direct correlation between the stiffness of the SFeS bonds as reflected by $k^a$ and the SFeS bond angle $\alpha$, as it is presented in the Supporting Information.

According to Table 3 and Figure 5a,b, the average stiffness of the SFeF bending mode for the selected chains in the ferric state of the protein ($k^a = 0.163$ mDyn/Å) is larger than in the gas phase ($k^a = 0.100$ mDyn/Å). Similarly, the average stiffness of the SFeS bending mode in the ferrous state of the protein ($k^a = 0.186$ mDyn/Å) is also larger than that in the gas phase ($k^a = 0.146$ mDyn/Å), which indicates that the protein environment increases the stiffness of this bending mode. The increased stiffness of SFeS bond bending can be explained by the fact that in the protein both methionines are connected to the protein back bone, which decreases the mobility of the move involving the side chains of both amino acids, and increases the SFeS bending mode stiffness relative to the gas phase. It is also interesting to note that the oxidation process of the protein decreases the stiffness of the SFeS bond bending (the average value of $k^a = 0.186$ and $0.163$ mDyn/Å, for the ferrous and ferric state, respectively), which is also consistent with the decreased values of the FeS bond strength (the average value of $k^a = 0.696$ and $0.436$ mDyn/Å, for the ferrous and ferric state, respectively).

## 4 | Conclusions

We investigated in this study the strength of the FeS bonds in the heme groups of AvBF for both the ferric and the ferrous oxidation states. For comparison, we used the related gas phase models to elaborate on the influence of the protein environment. The calculations of the protein were based on the QM/MM method, where we separately calculated each protein chain pair (AB, CD, EF, and GH) involving one heme group.

- The strength of the FeS bonds, as reflected by local FeS force constants, were correlated with their bond length, the energy density at a bond critical point, and the Fe and S atomic charges. In the ferric oxidation state of the protein, we found a good correlation between these properties for protein chain pairs AB, CD, and EF with the protein chain pair GH as an outlier. In the ferrous oxidation state we found a good correlation between these properties for the entire set of investigated FeS bonds. These results as well as the correlation between the local mode FeS force constants and the Fe and S charge differences, strongly indicate that a change of the oxidation state from ferrous to ferric, makes the FeS bonds more covalent and more polar.

- Overall, we found that in the ferric state, the strength of the FeS bonds of the protein is smaller than that in the gas phase, which is opposite to the ferrous state, where the FeS bonds are stronger than those in the gas phase. Therefore, according to our results, the protein environment plays a key role in the FeS bond strengths in the different oxidation states of the protein, which obviously is a key factor for the balance between these two states and the biological consequences thereof.

- For the majority of investigated protein chain pairs, we found a Badger type correlation between the FeS bond strength and the FeS bond length, which is in line with the general assumption that a stronger bond is generally a shorter one, which is not always the case as amply documented in the literature [70, 74, 95, 96]. The GH protein chain pair and the gas phase models in the ferric state, are other examples of the growing list of that exception.

- We investigated the SFeS bond angle and its stiffness, and found that the stronger FeS bond correlates with the more stiffer SFeS bond angle for both the ferric and the ferrous states. We also observed that the change from the ferric to ferrous oxidation state of the protein, generally increases the stiffness of the SFeS bond angle, which is consistent with the increase of the FeS bond strength.

In summary, our findings allow a better understanding of how heme-BF bonding plays an important role in the balance between the $Fe^{3+}$ and $Fe^{2+}$ ions in BF, explored at the molecular level. The results of this study will form a basis for subsequent studies on the impact of small molecular candidates being designed for a controlled manipulation of the balance between the ferric and ferrous oxidation states. We hope that our study will inspire our colleagues who are working on new antibiotics, to follow the new direction of the research, which is based on the iron imbalance in hemoproteins investigated in our study.

### Data Availability Statement

The data that supports the findings of this study are available in the Supporting Information of this article.

### References

1. G. Papanikolaou and K. Pantopoulos, "Iron Metabolism and Toxicity," *Toxicology and Applied Pharmacology* 202, no. 2 (2005): 199–211.

2. J. Liu, S. Chakraborty, P. Hosseinzadeh, et al., "Metalloproteins Containing Cytochrome, Iron–Sulfur, or Copper Redox Centers," *Chemical Reviews* 114, no. 8 (2014): 4366–4469.

3. B. Galy, M. Conrad, and M. Muckenthaler, "Mechanisms Controlling Cellular and Systemic Iron Homeostasis," *Nature Reviews Molecular Cell Biology* 25 (2024): 133–155.

4. D. Galaris and K. P. A. Barbouti, "Iron Homeostasis and Oxidative Stress: An Intimate Relationship," *BBA – Molecular Cell Research* 1866 (2019): 118535.

5. G. J. Anderson and D. M. Frazer, "Iron Homeostasis and Oxidative Stress: An Intimate Relationship," *American Journal of Clinical Nutrition* 106, no. Suppl (2017): 1559–1566S.

6. R. Eid, N. T. T. Arab, and M. T. Greenwood, "Iron Mediated Toxicity and Programmed Cell Death: A Review and a Re–Examination of Existing Paradigms," *Biochimica et Biophysica Acta* 1864, no. 2 (2017): 399–430.

7. E. Eren, N. R. Watts, F. Montecinos, and P. T. Wingfield, "Encapsulated Ferritin-Like Proteins: A Structural Perspective," *Biomolecules* 14 (2024): 624.

8. N. Dennis Chasteen and P. M. Harrison, "Mineralization in Ferritin: An Efficient Means of Iron Storage," *Journal of Structural Biology* 126, no. 3 (1999): 182–194.

9. K. J. Hintze and E. C. Theil, "Cellular Regulation and Molecular Interactions of the Ferritins," *Cellular and Molecular Life Sciences* 63, no. 5 (2006): 591–600.

10. K. H. Ebrahimi, P.-L. Hagedoorn, and W. R. Hagen, "Unity in the Biochemistry of the Iron–Storage Proteins Ferritin and Bacterioferritin," *Chemical Reviews* 115, no. 1 (2015): 295–326.

11. J. M. Bradley, N. E. Le Brun, and G. R. Moore, "Ferritins: Furnishing Proteins With Iron," *JBIC Journal of Biological Inorganic Chemistry* 21, no. 1 (2016): 13–28.

12. H. Yao, S. Alli, and L. Liu, "The Crystal Structure of *Acinetobacter Baumannii Bacterioferritin* Reveals a Heteropolymer of Bacterioferritin and Ferritin Subunits," *Nature Scientific Reports* 14 (2024): 18242.

13. S. Macedo, C. V. Romão, E. Mitchell, et al., "The Nature of the di-Iron Site in the Bacterioferritin From Desulfovibrio Desulfuricans," *Nature Structural & Molecular Biology* 10, no. 4 (2003): 285–290.

14. M. A. Carrondo, "Ferritins, Iron Uptake and Storage From the Bacterioferritin Viewpoint," *EMBO Journal* 22, no. 9 (2003): 1959–1968.

15. M. Rivera, "Bacterioferritin: Structure, Dynamics, and Protein–Protein Interactions at Play in Iron Storage and Mobilization," *Accounts of Chemical Research* 50, no. 2 (2017): 331–340.

16. A. N. D. Punchi, L. F. Hewage, J. Guidry, et al., "Mobilization of Iron Stored in Bacterioferritin Is Required for Metabolic Homeostasis in Pseudomonas Aeruginosa," *Pathogens* 9, no. 12 (2020): 980.

17. C. Jobichen, T. Y. Chong, R. Rattinam, et al., "Bacterioferritin Nanocage Structures Uncover the Biomineralization Process in Ferritins," *PNAS Nexus* 2, no. 7 (2023): 235.

18. E. Rosa-Núñez, C. Echavarri-Erasun, A. M. Armas, et al., "Iron Homeostasis in *Azotobacter Vinelandii*," *Biology* 12 (2023): 1423.

19. L. Swartz, M. Kuchinskas, H. Li, T. L. Poulos, and W. N. Lanzilotta, "Redox–Dependent Structural Changes in the *Azotobacter Vinelandii Bacterioferritin*: New Insights Into the Ferroxidase and Iron Transport Mechanism," *Biochemistry* 45, no. 14 (2006): 4421–4428.

20. M. A. Quail, P. Jordan, J. M. Grogan, et al., "Spectroscopic and Voltammetric Characterisation of the Bacterioferritin-Associated Ferredoxin Ofescherichia Coli," *Biochemical and Biophysical Research Communications* 229, no. 2 (1996): 635–642.

21. S. K. Weeratunga, C. E. Gee, S. Lovell, Y. Zeng, C. L. Woodin, and M. Rivera, "Binding of Pseudomonas Aeruginosa Apobacterioferritin–Associated Ferredoxin to Bacterioferritin b Promotes Heme Mediation of Electron Delivery and Mobilization of Core Mineral Iron," *Biochemistry* 48, no. 31 (2009): 7420–7431.

22. S. K. Weeratunga, S. Lovell, H. Yao, et al., "Structural Studies of Bacterioferritin b From Pseudomonas Aeruginosa Suggest a Gating Mechanism for Iron Uptake via the Ferroxidase Center," *Biochemistry* 49, no. 6 (2010): 1160–1175.

23. S. Yasmin, S. C. Andrews, G. R. Moore, and N. E. Le Brun, "A New Role for Heme, Facilitating Release of Iron From the Bacterioferritin Iron Biomineral," *Journal of Biological Chemistry* 286, no. 5 (2011): 3473–3483.

24. S. G. Wong, R. Abdulqadir, N. E. Le Brun, G. R. Moore, and A. G. Mauk, "Fe–Haem Bound to Escherichia Coli Bacterioferritin Accelerates Iron Core Formation by an Electron Transfer Mechanism," *Biochemical Journal* 444, no. 3 (2012): 553–560.

25. H. Yao, Y. Wang, S. Lovell, et al., "The Structure of the BfrB–Bfd Complex Reveals Protein–Protein Interactions Enabling Iron Release From Bacterioferritin," *Journal of the American Chemical Society* 134, no. 32 (2012): 13470–13481.

26. Y. Wang, H. Yao, Y. Cheng, et al., "Characterization of the Bacterioferritin/Bacterioferritin Associated Ferredoxin Protein–Protein Interaction in Solution and Determination of Binding Energy Hot Spots," *Biochemistry* 54, no. 40 (2015): 6162–6175.

27. G. Khare, P. Nangpal, and A. K. Tyagi, "Differential Roles of Iron Storage Proteins in Maintaining the Iron Homeostasis in Mycobacterium Tuberculosis," *PLoS One* 12, no. 1 (2017): e0169545.

28. A. N. D. Punchi, Y. H. Yao, B. Nammalwar, et al., "Small Molecule Inhibitors of the Bfrb–Bfd Interaction Decrease Pseudomonas Aeruginosa Fitness and Potentiate Fluoroquinolone Activity," *Journal of the American Chemical Society* 141, no. 20 (2019): 8171–8184.

29. J. Pullin, J. M. Bradley, G. R. Moore, N. E. Le Brun, M. T. Wilson, and D. A. Svistunenko, "Electron Transfer From Haem to the di–Iron Ferroxidase Centre in Bacterioferritin," *Angewandte Chemie, International Edition* 60, no. 15 (2021): 8376–8379.

30. A. Mohanty, A. Parida, B. Subhadarshanee, et al., "Alteration of Co-axial Heme Ligands Reveals the Role of Heme in Bacterioferritin From Mycobacterium Tuberculosis," *Inorganic Chemistry* 60, no. 22 (2021): 16937–16952.

31. A. Soldano, H. Yao, and A. N. D. Punchi-Hewage, "Small Molecule Inhibitors of the Bacterioferritin (Bfrb)–ferredoxin (Bfd) Complex Kill Biofilm-Embedded Pseudomonas Aeruginosa Cells," *ACS Infectious Diseases* 7, no. 1 (2021): 123–140.

32. H. Yao, A. Soldano, L. Fontenot, et al., "Pseudomonas Aeruginosa Bacterioferritin Is Assembled From Ftna and Bfrb Subunits With the Relative Proportions Dependent on the Environmental Oxygen Availability," *Biomolecules* 12, no. 3 (2022): 366.

33. A. M. van der Ven, H. Gyamfi, U. Suttisansanee, et al., "Molecular Engineering of e. Coli Bacterioferritin: A Versatile Nanodimensional Protein Cage," *Molecules* 28, no. 12 (2023): 4663.

34. M. Rivera, "Mobilization of Iron Stored in Bacterioferritin, a New Target for Perturbing Iron Homeostasis and Developing Antibacterial and Antibiofilm Molecules," *Journal of Inorganic Biochemistry* 247 (2023): 112306.

35. A. Dautant, J.-B. Meyer, J. Yariv, G. Précigoux, and R. M. Sweet, "A. Joseph Kalb (Gilboa), and Felix Frolow. Structure of a Monoclinic Crystal Form of Cytochrome b1 (Bacterioferritin) From e. Coli," *Acta Crystallographica Section D* 54, no. 1 (1998): 16–24.

36. C. E. Tzeliou, M. A. Mermigki, and D. Tzeli, "Review on the QM/MM Methodologies and Their Application to Metalloproteins," *Molecules* 27, no. 9 (2022): 2660.

37. M. W. van der Kamp and A. J. Mulholland, "Combined Quantum Mechanics/Molecular Mechanics (QM/MM) Methods in Computational Enzymology," *Biochemistry* 52 (2013): 2708–2728.

38. V. Guallar and F. H. Wallrapp, "QM/MM Methods: Looking Inside Heme Proteins Biochemisty," *Biophysical Chemistry* 149, no. 1 (2010): 1–11.

39. A. Warshel and M. Levitt, "Theoretical Studies of Enzymic Reactions: Dielectric, Electrostatic and Steric Stabilization of the Carbonium Ion in the Reaction of Lysozyme," *Journal of Molecular Biology* 103, no. 2 (1976): 227–249.

40. A. Warshel and M. Karplus, "Calculation of Ground and Excited State Potential Surfaces of Conjugated Molecules. i. Formulation and Parametrization," *Journal of the American Chemical Society* 94, no. 16 (1972): 5612–5625.

41. E. Kraka, W. Zou, and Y. Tao, "Decoding Chemical Information From Vibrational Spectroscopy Data: Local Vibrational Mode Theory," *WIREs Computational Molecular Science* 10 (2020): 1480.

42. E. Kraka, M. Quintano, H. W. La Force, J. J. Antonio, and M. Freindorf, "The Local Vibrational Mode Theory and Its Place in the Vibrational Spectroscopy Arena," *Journal of Physical Chemistry. A* 126 (2022): 8781–8798.

43. R. F. W. Bader, "The Quantum Mechanical Basis of Conceptual Chemistry," *Monatshefte für Chemie* 136, no. 6 (2005): 819–854.

44. R. F. W. Bader, *Atoms in Molecules: A Quantum Theory (International Series of Monographs on Chemistry)* (Oxford, England: Clarendon Press, 1994).

45. R. F. W. Bader, "A Quantum Theory of Molecular Structure and Its Applications," *Chemical Reviews* 91, no. 5 (1991): 893–928.

46. A. E. Reed, L. A. Curtiss, and F. Weinhold, "Intermolecular Interactions From a Natural Bond Orbital, Donor-Acceptor Viewpoint," *Chemical Reviews* 88 (1988): 899–926.

47. F. Weinhold and C. R. Landis, *Valency and Bonding: A Natural Bond Orbital Donor-Acceptor Perspective* (England: Cambridge University Press, 2005).

48. D. A. Case, I. Y. Ben-Shalom, S. R. Brozell, et al., *Amber* (San Francisco: University of California, 2018).

49. W. L. Jorgensen, J. Chandrasekhar, J. D. Madura, R. W. Impey, and M. L. Klein, "Comparison of Simple Potential Functions for Simulating Liquid Water," *Journal of Chemical Physics* 79, no. 2 (1983): 926–935.

50. D. A. Giammona, *An Examination of Conformational Flexibility in Porphyrins and Bulky-Ligand Binding in Myoglobin*. PhD thesis, (Davis: University of California, 1984).

51. L. W. Chung, W. M. C. Sameera, R. Ramozzi, et al., "The ONIOM Method and Its Applications," *Chemical Reviews* 115 (2015): 5678–5796.

52. T. Vreven and K. Morokuma, "Hybrid Methods: ONIOM(QM:MM) and QM/MM," in *Annual Reports in Computational Chemistry* (Spellmeyer, D.C. editor: Elsevier, 2006).

53. K. Thom Vreven, S. Byun, I. Komáromi, et al., "Combining Quantum Mechanics Methods With Molecular Mechanics Methods in ONIOM," *Journal of Chemical Theory and Computation* 2, no. 3 (2006): 815–826.

54. C. Adamo and V. Barone, "Toward Reliable Density Functional Methods Without Adjustable Parameters: The PBE0 Model," *Journal of Chemical Physics* 110, no. 13 (1999): 6158–6170.

55. R. Ditchfield, W. J. Hehre, and J. A. Pople, "Self–Consistent Molecular–Orbital Methods. IX. An Extended Gaussian–Type Basis for Molecular–Orbital Studies of Organic Molecules," *Journal of Chemical Physics* 54 (1971): 724–728.

56. Y. Ran, H. Zhu, M. Liu, et al., "Bis-Methionine Ligation to Heme Iron in the Streptococcal Cell Surface Protein Shp Facilitates Rapid Hemin Transfer to HtsA of the HtsABC Transporter," *Journal of Biological Chemistry* 282, no. 43 (2007): 31380–31388.

57. S. Zhao, Z.-H. Li, W.-N. Wang, et al., "Is the Uniform Electron Gas Limit Important for Small Ag Clusters? Assessment of Different Density Functionals for $Ag_n$ (n¡4)," *Journal of Chemical Physics* 124, no. 18 (2006): 184102.

58. C. J. Cramer and D. G. Truhlar, "Density Functional Theory for Transition Metals and Transition Metal Chemistry," *Physical Chemistry Chemical Physics* 11, no. 46 (2009): 10757–10816.

59. S. Li, J. M. Hennigan, D. A. Dixon, and K. A. Peterson, "Accurate Thermochemistry for Transition Metal Oxide Clusters," *Journal of Physical Chemistry. A* 113, no. 27 (2009): 7861–7877.

60. M. Freindorf and E. Kraka, "Critical Assessment of the FeC and CO Bond Strength in Carboxymyoglobin - A QM/MM Local Vibrational Mode Study," *Journal of Molecular Modeling* 26 (2020): 1–15.

61. P. Rydberg and L. Olsen, "The Accuracy of Geometries for Iron Porphyrin Complexes From Density Functional Theory," *Journal of Physical Chemistry. A* 113, no. 43 (2009): 11949–11953.

62. M. K. Safo, G. P. Gupta, F. Ann Walker, and W. Robert Scheidt, "Models of the Cytochromes b. Control of Axial Ligand Orientation With a Hindered Porphyrin System," *Journal of the American Chemical Society* 113, no. 15 (1991): 5497–5510.

63. D. Cremer and E. Kraka, "From Molecular Vibrations to Bonding, Chemical Reactions, and Reaction Mechanism," *Current Organic Chemistry* 14 (2010): 1524–1560.

64. E. Kraka, J. A. Larsson, and D. Cremer, "Generalization of the Badger Rule Based on the Use of Adiabatic Vibrational Modes," in *Computational Spectroscopy*, ed. J. Grunenberg (New York: Wiley, 2010), 105–149.

65. I. Mayer, "Charge, Bond Brder an Valence in the Ab Initio Theory," *Chemical Physics Letters* 97 (1983): 270–274.

66. I. Mayer, "Bond Orders and Valences From Ab Initio Wave Functions," *International Journal of Quantum Chemistry* 29 (1986): 477–483.

67. I. Mayer, "Bond Order and Valence Indices: A Personal Account," *Journal of Computational Chemistry* 28, no. 1 (2007): 204–221.

68. E. Bright Wilson, "Some Mathematical Methods for the Study of Molecular Vibrations," *Journal of Chemical Physics* 9 (1941): 76–84.

69. Z. Konkoli and D. Cremer, "A New Way of Analyzing Vibrational Spectra. I. Derivation of Adiabatic Internal Modes," *International Journal of Quantum Chemistry* 67 (1998): 1–9.

70. Z. Konkoli, J. A. Larsson, and D. Cremer, "A New Way of Analyzing Vibrational Spectra. II. Comparison of Internal Mode Frequencies," *International Journal of Quantum Chemistry* 67 (1998): 11–27.

71. E. Wilson, J. Decius, and P. Cross, *Molecular Vibrations: The Theory of Infrared and Raman Vibrational Spectra* (New York: McGraw-Hill, 1955).

72. V. Barone, S. Alessandrini, M. Biczysko, et al., "Computational Molecular Spectroscopy," *Nature Reviews Methods Primers* 1, no. 1 (2021): 38.

73. W. Zou and D. Cremer, "Properties of Local Vibrational Modes: The Infrared Intensity," *Theoretical Chemistry Accounts* 133 (2014): 1451–1466.

74. Z. Konkoli and D. Cremer, "A New Way of Analyzing Vibrational Spectra. III. Characterization of Normal Vibrational Modes in Terms of Internal Vibrational Modes," *International Journal of Quantum Chemistry* 67 (1998): 29–40.

75. Z. Konkoli, J. A. Larsson, and D. Cremer, "A New Way of Analyzing Vibrational Spectra. IV. Application and Testing of Adiabatic Modes Within the Concept of the Characterization of Normal Modes," *International Journal of Quantum Chemistry* 67 (1998): 41–55.

76. N. Verma, Y. Tao, W. Zou, et al., "A Critical Evaluation of Vibrational Stark Effect (VSE) Probes With the Local Vibrational Mode Theory," *Sensors* 20 (2020): 2358.

77. R. T. Moura, Jr., M. Quintano, J. J. Antonio, M. Freindorf, and E. Kraka, "Automatic Generation of Local Vibrational Mode Parameters: From Small to Large Molecules and QM/MM Systems," *Journal of Physical Chemistry. A* 126 (2022): 9313–9331.

78. M. Quintano, A. A. A. Delgado, R. T. Moura Jr, M. Freindorf, and E. Kraka, "Local mode analysis of characteristic vibrational coupling in nucleobases and Watson–Crick base pairs of DNA," *Electronic Structure* 4, no. 12 (2022): 44005.

79. M. Quintano, R. T. Moura Jr, and E. Kraka, "Frontier Article: Local Vibrational Mode Theory Meets Graph Theory: Complete and Non–Redundant Local Mode Sets," *Chemical Physics Letters* 849 (2024): 141416.

80. W. Zou and D. Cremer, "$C_2$ in a Box: Determining Its Intrinsic Bond Strength for the X1 $\Sigma_g^+$ Ground State," *Chemistry - A European Journal* 22 (2016): 4087–4099.

81. M. Freindorf, A. A. A. Delgado, and E. Kraka, "CO Bonding in Hexa– and Pentacoordinate Carboxy–Neuroglobin – A QM/MM and Local Vibrational Mode Study," *Journal of Computational Chemistry* 43 (2022): 1725–1746.

82. A. Madushanka, N. Verma, M. Freindorf, and E. Kraka, "Papaya Leaf Extracts as Potential Dengue Treatment: An in-Silico Study," *International Journal of Molecular Sciences* 23 (2022): 12310.

83. J. J. Antonio and E. Kraka, "Non-covalent $\pi$–Interactions in Mutated Aquomet-Myoglobin Proteins: A QM/MM and Local Vibrational Mode Study," *Biochemistry* 62 (2023): 2325–2337.

84. M. Freindorf, J. Antonio, and E. Kraka, "Hydrogen Sulfide Ligation in Hemoglobin I of *Lucina Pectinata* – A QM/MM and Local Mode Study," *Journal of Physical Chemistry. A* 127 (2023): 8316–8329.

85. M. Freindorf, J. Antonio, and E. Kraka, "Iron–Histidine Bonding in Bishistidyl Hemoproteins – A Local Vibrational Mode Study," *Journal of Computational Chemistry* 45 (2024): 574–588.

86. Y. Dangat, M. Freindorf, and E. Kraka, "Mechanistic Insights Into SDepalmitolyse Activity of Cln5 Protein Linked to Neurodegeneration and Batten Disease: A QM/MM Study," *Journal of the American Chemical Society* 146 (2024): 145–158.

87. D. Cremer and E. Kraka, "Chemical Bonds Without Bonding Electron Density? Does the Difference Electron-Density Analysis Suffice for a Description of the Chemical Bond?," *Angewandte Chemie, International Edition* 23 (1984): 627–628.

88. D. Cremer and E. Kraka, "A Description of the Chemical Bond in Terms of Local Properties of Electron Density and Energy," *Croatica Chemica Acta* 57 (1984): 1259–1281.

89. F. Weinhold, C. R. Landis, and E. D. Glendening, "What Is NBO Analysis and How Is It Useful?," *International Reviews in Physical Chemistry* 35, no. 3 (2016): 399–440.

90. M. J. Frisch, G. W. Trucks, H. B. Schlegel, et al., *Gaussian 16* (Wallingford CT: Gaussian Inc, 2016).

91. W. Zou, R. M. Jr, M. Quintano, et al., "LModeA2023," in *Computational and Theoretical Chemistry Group (CATCO), Southern Methodist University* (Dallas, TX, USA: Southern Methodist University, 2023).

92. T. A. Keith, "AIMAll (Version 19.10.12), TK Gristmill Software," 2019.

93. R. M. Badger, "A Relation Between Internuclear Distances and Bond Force Constants," *Journal of Chemical Physics* 2 (1934): 128–131.

94. J. J. Antonio and E. Kraka, "Metalring Interactions in Group 2 Ansa-Metallocenes: Assessed With the Local Vibrational Mode Theory," *Physical Chemistry Chemical Physics* 26 (2024): 15143–15155.

95. E. Kraka and D. Cremer, "Characterization of CF Bonds With Multiple-Bond Character: Bond Lengths, Stretching Force Constants, and Bond Dissociation Energies," *ChemPhysChem* 10 (2009): 686–698.

96. M. Kaupp, D. Danovich, and S. Shaik, "Chemistry Is About Energy and Its Changes: A Critique of Bond-Length/Bond-Strength Correlations," *Coordination Chemistry Reviews* 344 (2017): 355–362.

## Supporting Information

Additional supporting information can be found online in the Supporting Information section.